



A Novel Four legged linear piezoelectric inchworm motor with high thrust force

Sandip Jana^{1,2} · Saikat Kumar Shome^{1,2} · Arup Kumar Nandi^{1,2}

Received: 4 April 2024 / Accepted: 1 July 2024

© The Author(s), under exclusive licence to Springer-Verlag GmbH Germany, part of Springer Nature 2024

Abstract

A major limitation of most linear motors is limited travel range and low load capacity. In this research, a large motion range piezoelectric Inchworm Motor (IM) is realised which not only harnesses the prominent advantages of piezo-actuator but the four-legged design simultaneously offers reliable self-locking capability in a compact form-factor. The displacement deformation of each element of the motor (clamps, extender) is determined using finite element analysis (FEA) through force distribution analysis. Appropriate clamping force adjustment method on the rail/stator of the motor is adopted using load cell followed by multiple linear regression modelling to dynamically consider the clamping force and inherent non-linearities of piezo-actuators (PAs). The hardware prototype is fabricated and the experiment results verify the validity of the data driven model. Clamping error analysis, step length dependent stability profile and dynamic driving force has been carried out to characterize the IM. Performance evaluation of the motor has been researched at different voltages, frequencies and loads to assess its operating profile. Mechanical output suggests that the prototype achieves a maximum no load speed of 39.64 mm/sec under clamping force of 2 N at 100 V and frequency of 2000 Hz with 30% duty cycle. With load of 700 g, 0.46 mm/sec speed is obtained under a clamping force of 8 N. In addition, bidirectional control signal mechanism for the IM has been also developed, tested and implemented in real-time environment. The proposed large driving force prototype designed is highly suitable for industrial linear translation systems requiring high resolution, large strokes, and heavy loads capacities.

1 Introduction

Piezoelectric actuators are widely used in fields such as biomedical engineering, semiconductor manufacturing, optical focusing and scanning microscopy because of their compact size, large output force, rapid response, high electromechanical coupling efficiency, high blocking force capability and high resolution. In addition to achieving high position accuracy, another advantage of piezoelectric actuator is its small volume and low thermal expansion coefficient during motion. Various types of piezoelectric actuators can be classified according to their working principles, such as ultrasonic actuators, direct driving actuators, inchworm actuators, stick–slip actuators.

Actuators with direct drive offer high resolution but have a limited working stroke while ultrasonic actuator generates large motion but considers heat generation issues. The maximum output thrust capability of inchworm motor is greater than stick slip piezo-actuator, however the control and drive systems are more complicated.

For piezo-actuators, several frameworks are available in literature which provides specific mathematical formulations leading to model-based control design. An equivalent circuit based dynamic model was proposed by Dong et al. to describe electrical behaviour of the actuator (Devasia et al. 2007). Since nonlinear system parameters such as friction and hysteresis contribute to the complexity of mathematical model of piezo-based motor, a data-driven approach would be a better alternative. Different data driven techniques such as single source and dual source dual frequency (DSDF) approach is adopted for piezoelectric ultrasonic motor in Makarem et al. (2021) wherein the experimental data are collected from the real plant to approximate the mathematical modelling and modeling of

✉ Saikat Kumar Shome
saikatshome@cmeri.res.in

¹ CSIR—Central Mechanical Engineering Research Institute, Durgapur 713209, India

² Academy of Scientific and Innovative Research (AcSIR), Ghaziabad 201002, India

hand manipulator using data driven approach in Sintov et al. (2020).

For a long time, major focus has been on development of actuators made from smart materials instead of traditional linear motors, specifically for micron-level positioning, active vibration control, etc. To address the existing gap between smart material produced displacement and need for long stroke driving, it is critical to deliver and accumulate the deformation of these materials in a controlled and precise manner. Of late, researchers have discovered that an inchworm-based motion principle can be applied to build a linear motor by accumulating steps in order to generate cumulative infinite distance which is specifically relevant to precise long-distance application along with a compact form factor. Considerable research has been carried out in the last decade to design inchworm motion principle using electrostatic, electro thermal and piezoelectric motors to improve the output force, high switching driving and positioning capability (Joshi 2020; Kim et al. 2002; Cusin et al. 2000; Yang et al. 2006).

A novel electrostatic IM with flexible drive arms has been developed, manufactured and tested for high force density in Penskiy et al. (2011) where flexible drive arm enables the shuttle to move longitudinally by converting transverse motion of the inchworm. The motor achieved a maximum speed 3.6 mm/sec under the locking force of 0.7 mN and driving voltage of 110 V. To improve output force density of the motor, a new architecture for in-plane electrostatic gap-closing actuators along with flexible driving arms and a single mask fabrication is proposed in Penskiy and Bergbreiter 2013, where the motor demonstrated maximum force of 1.88 mN at driving voltage of 110 V and achieved a force density of 1.38 mN/mm². A screw clamp principle-based hybrid linear actuator is proposed (Shi et al. 2021) along with two clamping nuts and cylindrical piezo electric stack symmetrically placed at two ends of the actuator and rotor as a feed screw assembled throughout all the parts. Proposed motor is fabricated for experimental analysis and achieved a maximum no load speed 20 mm/sec under maximum output thrust of 280 N. A three piezo-actuator based high force linear IM for structural shape control is proposed in Galante et al. (1998) with displacement range and force handling capabilities of 6 mm, 200 N respectively, attaining a maximum velocity of 5.4 mm/sec with a driving sinusoidal signal of 900 Hz. A right circular mechanism-based stick–slip piezoelectric actuator is proposed in Cheng et al. (2017) to obtain linear motion wherein a slider moves by motion of the stick–slip actuator. Maximum load handling capacity of the prototype is 3 N at a speed of 5.96 mm/sec. Thus, it is observed from the reported PZT based inchworm motor literature that although developed motors are capable to sustain large

driving force actuation capabilities along with high material internal stress yet the primary challenge lies in high frequency operation.

The clamping mechanism also plays a crucial role in determining the feasibility of PZT based inchworm motor. Hence, the design and fabrication of more efficient clamping mechanisms remains a core concern for piezo based IM. The inchworm motor mechanism is directly affected by the clamping mechanism both in terms of precision positioning and force capacity. In spite of the fact that researchers are more focused of the importance of clamping mechanism during design of the IM, however it is designed to address the driving ability and inherent problem of nonlinear parameters such as hysteresis (Calkins et al. 2000), frictional force (Pan et al. 2017), heat (Yamamoto et al. 1999), etc.

PAs research has produced many successes, but the majority of these have been aimed at low- and medium-frequency actuation. Conventionally, the driving principle of intermediate and high-frequency piezo-actuators uses stator resonance to generate the large displacement, and thus generating large motion using the frictional/clamping force of stator. Most of the literature reports low frequency driving mechanisms such as a piezoelectric MEMS vibration energy harvester proposed by Nabavi et al. (Nabavi and Zhang 2018) works at a low resonant frequency of less than 200 Hz. Another low frequency piezo electric motor is proposed by Xing et al. based on a piezoelectric driving mechanism and magnetic modulation. Motor operated at a modest frequency of 3 Hz and at 4.5 V driving voltage which generates a speed of 0.1104 rad/min (Xing and Qin 2020). Resonant type piezoelectric motors can produce large strokes and high speeds by operating at ultrasonic frequencies. However, their main drawback is reduced resolution. Therefore, a non-resonant type piezo motor with precise driving ability is proposed (Xu et al. 2018) where runners are pushed step-by-step by a hybrid motion created by two bending motions of a sandwich transducer. A no load velocity 5.96 μ m/sec is achieved under the frequency of 400 Hz with a maximum thrust of 30 N.

As evident from the discussed prior arts, one of the important mechanical characteristics of the piezo-based inchworm motor is that operational speed is limited in nature and motors do not exhibit a high driving frequency and output thrust, limiting their use for high-speed linear translation application. In order to increase the displacement and speed of the extending device, the motor should be operated at higher frequencies.

The present research describes the development and testing of a four-legged piezo based inchworm motor with high force driving capability. The contribution of the work can be summarized as: (i) Mechanical design and fabrication of four legged inchworm motor with force distribution analysis of each element (clamps, extender) using FEM.

(ii) Development of data driven model to verify the motion of the extender at different frequencies, (iii) Investigation of IM characteristic through experimental study of clamping error, step length stability and dynamic driving force, (iv) Experimental investigation towards performance evaluation of inchworm motor with varying operating voltages, switching frequencies and loads under different clamping forces, (v) Development of bidirectional motion logic of the proposed motor in real time environment.

This paper is organized into six sections as follows. The operating principle of inchworm mechanism, design of the motor, study of force distribution analysis for each of its component using FEM method and clamping force measurement are described in Section II. The data driven model to verify the motion of the IM is discussed in section III. Section IV describes the experimental system for the prototype, characterization of the IM and performance analysis of the proposed system under different clamping force. Bidirectional operations under different frequencies are illustrated in section V.

2 Mechanical structure & IM operating principle

2.1 Operating principle of four legged piezoelectric IM

Operating mechanism of the proposed piezo electric motor is sequentially discussed in Fig. 1a and the corresponding

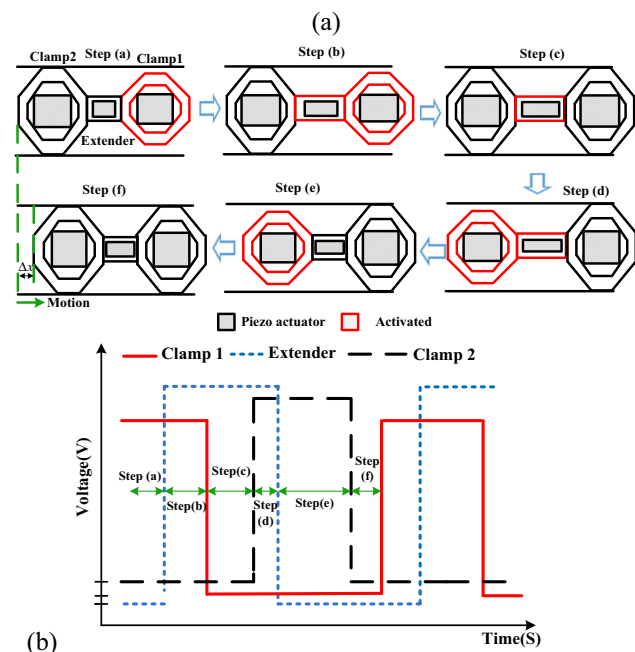


Fig. 1 a IM operating mechanism comprising six steps b Motion generation voltage curve for IM during single cycle

voltage control waveform for generating motion during a specific time period is illustrated in Fig. 1b. Clamp 1 and clamp 2 control pulses are 180 degrees phase shifted from each other and the extender is 30 degrees phase shifted from clamp 1. The inchworm mechanism comprises three piezoelectric actuators built into the mechanical structure of the motor; two of them act as “clamps”, while the third one acts as an “extender.” The actual displacement of the motor is achieved by extension of the extender which comprises a series of clamping and extending mechanism through six steps to get the desired displacement. The motor ensures full clamping abilities when it is not activated, that is at the resting condition (step (f)) where both clamping actuators of the motor (clamp 1, clamp 2) are not excited and remain closed (in contact with the stator). In the first step (a) of six step cycles, clamp 1 is ON which releases it from the stator (gap between stator and rotor). Then, extender is energized by driving signal and it moves along a linear path (step (b)). In the third step (c) closing of clamp 1 takes place and this completes the first half of the six stepped cycle. In fourth step (d), clamp 2 is activated which releases its contact from the stator followed by turning off the extender in step(e) which restores it back to its original length. In the last step (f), clamp 2 is deactivated which causes definite displacement of motor at the end of six steps. It is important to note that in part of inchworm operation principle, the extender accumulates small displacements that add up to a large displacement (Δx).

During a typical inchworm cycle, only one clamping device is triggered at a time, which allows the extender to expand and retract without inhibition. Purpose of the clamping structures is to create a frictional force that can resist static forces resulting from a constant load generated from the extending mechanism. In our study, four-legged inchworm linear motor has been developed where four piezo stack actuators are used as clamps which act as four legs for the motor, as shown in Fig. 2. Speed of the motor depends on the step size and the rate at which the cycle repeats i.e. driving frequency and is calculated as the net displacement travelled in the given time, derived as step size \times driving frequency.

2.2 Piezo-actuator (PAs) characteristic

It’s critical to select the correct PAs, since displacement reduction is an integral part of actuator force generation. Therefore, stiffness of the mechanical structure of IM must be linked to the PAs force/displacement curves. Based on the stiffness of the Clamping Mechanism (CM) and Extending Mechanism (EM), Noliac PAs have been chosen for the current research. NAC 2013 H10 and NAC 2013

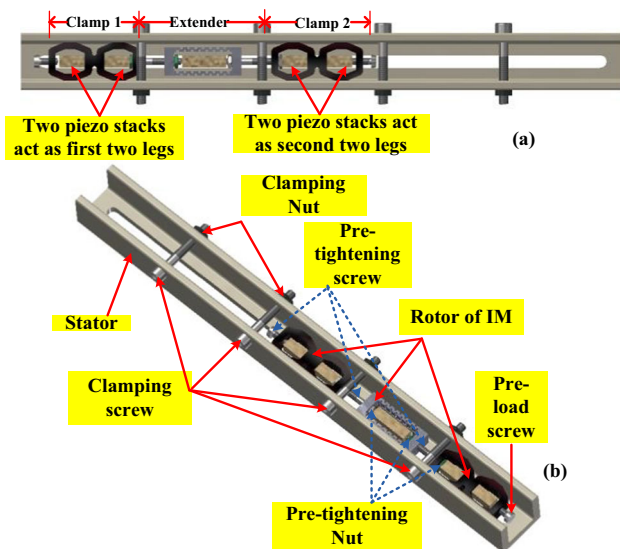


Fig. 2 Proposed piezo based IM design structure with self-locking at rest capability **a** top view, **b** 3D model

H20 are used for clamps and extender whose specification is tabulated in Table 1.

2.3 Prototype development and force distribution analysis of the IM

The research paper proposes an IM design illustrated in Fig. 2.

Motor consists of a rotor (moving component) which includes two CMs (black) as well as an EM (gray). Five PAs (mustard) are inserted into the CMs and EM and a pre-tightening screw is used to connect the CM and EM. To maintain a uniform clamping force on the rotor, clamping screws are equipped with clamping nuts as shown in Fig. 2b. It is assumed that there is no gap between the rotor and stator and the non-linearity in the PA system is ignored. The motor’s rotor is connected to the stator through a screw, and the rotor is locked with the stator when the motor is powered off which ensures full clamping capability at rest. To unlock CM from the stator, the PAs in the CM need to be activated.

Mechanical design solves difficulties linked with specific integration constraints and motor clamping force requirements. In this design, the connection between CMs and EM of the motor is adjusted by screws, nuts and coupler. Metallic chips are used to adjust the piezo actuator in the clamps and extender structure. The length of the

rotor can be adjusted by increase and decrease of the connecting coupler between the clamp and extender.

An asymmetrical flexure hinge mechanism structure of the extender has been proposed which increases static friction force during slow extension stage and reduces the kinetic friction force in quick contraction stage by the linear driving motion of the extenders piezo actuator as shown in Fig. 3b). Additionally, the specific design dissipates heat quickly to the surrounding. The clamp is designed as an octagon structure to ensure full clamping abilities at rest condition as well as to generate frictional force that can withstand both static and dynamic forces. The three individual parts (clamp 1, extender, clamp 2) of the inchworm motor which have been designed and fabricated as shown in Fig. 3a, b are then assembled with the piezo-actuator to implement the complete motor (IM) as shown in Fig. 3c. Two piezo-actuators are fitted into each of the clamps of the motor and one piezo-actuator is fixed into the extender structure. The total outer length, width and height of the clamps are 40 mm, 17 mm and 7 mm respectively while the inner length and width are 12 mm, 10 mm respectively. Similarly, the outer length, width and height of mechanical structure of extender are 34 mm, 12 mm and 7 mm respectively. Prototype of the complete motor has been manufactured with a dimension of $114 \times 17 \times 7 \text{ mm}^3$ (without screw and coupler) for rail and $250 \times 24 \times 20 \text{ mm}^3$ for the stator. It is machined with a tolerance value of $\pm 0.1 \text{ mm}$ and all parts of the motor are made of stainless steel (clamps, extender).

To compute performance of the clamp and extender of inchworm motor, 3D FEA has been conducted using ANSYS software. The clamping unit ensures full clamping ability when it is deactivated and initially locked on the rail or stator through clamping screw equipped with nuts and spring. To meet the requirements for clamp stiffness, the clamp’s length, width, and thickness have been varied using steel as the material for rotor/stator having density of 7862 kg/m^3 , elastic modulus of 230 GPa and Poisson ratio of 0.28. The clamps generate displacement of $\pm 6.67 \text{ }\mu\text{m}$ along X-axis and $\pm 2.39 \text{ }\mu\text{m}$ along Y-axis on applying 650 N force into the piezo-actuator which activates the clamping mechanism of the motor as seen in Fig. 4a. Thus, a PA with stiffness of $97.45 \text{ N}\mu\text{m}^{-1}$ is needed.

Extending unit ensures actuation of the extender of inchworm which in turn controls the speed and produces the required driving force to be generated by the motor. To increase motion range, a high value capacitive piezo-

Table 1 Specification of piezoelectric stack actuator used in the IM

Type	Dimensions [mm^3]	Free stroke [μm]	Blocking force [N]	Capacitance [μF]
CM: NAC2013H10	$5 \times 5 \times 10$	13.2	1050	0.72
EM: NAC2013-H20	$5 \times 5 \times 20$	29.7	1050	1.62

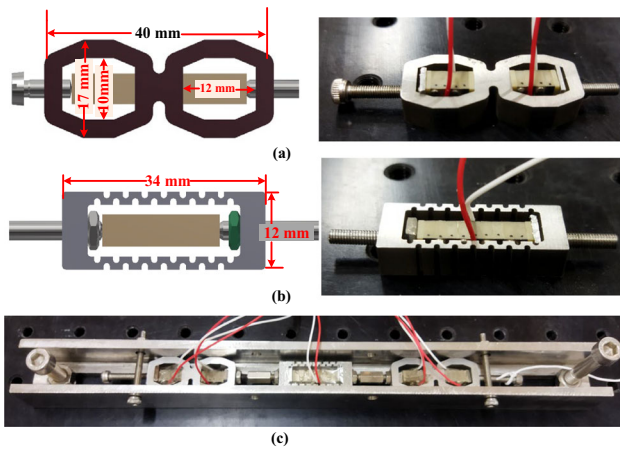


Fig. 3 Individual parts IM prototype—**a** CMs **b** EM **c** assembly of the different components (clamps, extender) including PZT stacks to form complete IM motor

actuator is needed for extender as piezo capacitance is a function of the excitation voltage frequency. Simulated displacement variation in response to applied force of 850 N on the PZA along X-axis is shown in Fig. 5a where displacement of 14.81 μm along X-axis is obtained. Therefore, stiffness of the extender is found to be 57.39 $\text{N } \mu\text{m}^{-1}$. Figure 5b shows the Von-Mises stress of the extending mechanism which is lower than the yield stress of the constitutive material (250 Mpa). Based on the stiffness of the inchworm mechanical structure, appropriate PA has been chosen according to the generated force, displacement, and dimensions.

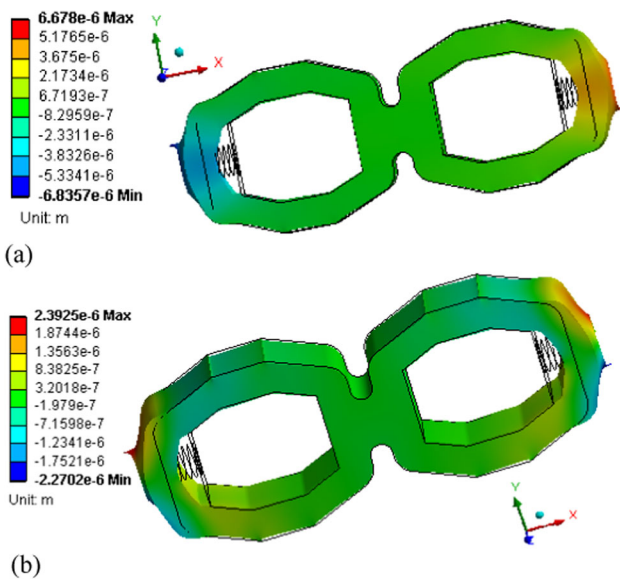


Fig. 4 Displacement distribution of the CMs **a** X-axis **b** Y-axis

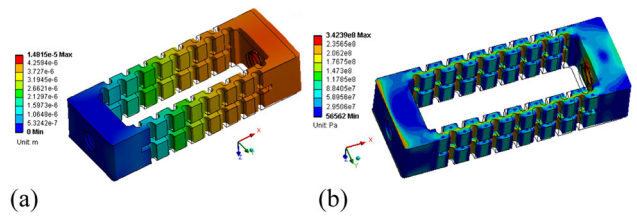


Fig. 5 **a** Displacement distribution of the EM along X-axis (3D view) **b** Von misses stress analysis of extending mechanism along X-axis

2.4 Clamping force measurement by load cell

It is considered that tangential frictional force is equal to the normal force applied to the stator by the moving rotor of the motor. Therefore, in order to determine the clamping force imposed on the stator, a compression testing machine (CTM) is used for experiments. Figure 6 provides an illustration of the method to determine the imposed clamping force using a load cell (LCM 100) and CTM machine. The load cell is operated by 14 Volt input supply which is fitted into stator and connecting the load cell amplifier to digital storage oscilloscope (DSO) and the amplified output voltage change in term of force is then measured in DSO via the load cell amplifier. Force is generated when the load cell is compressed by clamping force (frictional force) acting on the stator of the motor. The applied clamping force on the rail of the motor through screw is measured using calibrated voltage-force data. The experimental setup for determining the clamping force measurement is shown in Fig. 6 and voltage deviation vs time plot is shown in Fig. 7a. A plot of clamping force vs voltage deviation graph shows that the voltage deviation and clamping force has a linear relationship as illustrated in Fig. 7b.

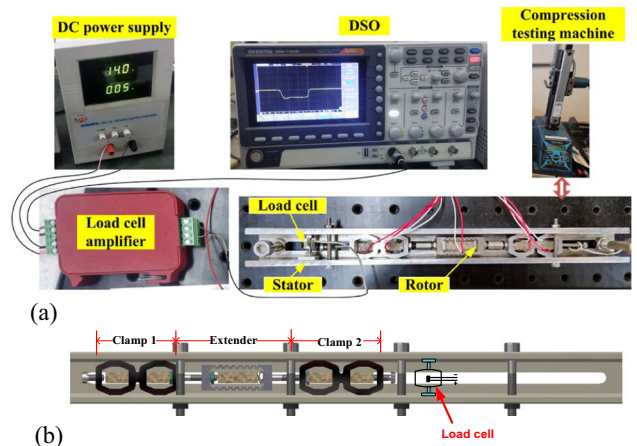


Fig. 6 **a** Experimental set up for measurement of clamping force on the stator through load cell **b** Schematic diagram of load cell position in the inchworm motor

2.5 High switching frequency inchworm motor drive

High frequency driver circuit has been designed to actuate the proposed IM which includes MOSFET based switching circuit (MSC) and oscillation circuit. 24 V Battery signal has been amplified to attain the desired voltage signal to operate the piezoelectric actuators through necessary electrical balancing and high switching operation, as discussed in Fig. 8.

3 Data driven modeling

Mathematical modelling of the piezo based inchworm motor is used instead of model based controller which is difficult to implement due to non-linearity of the system. The main non linearity of the piezo based inchworm motor is the clamping force which is affected by several operational factors such as frequency and velocity of operation, temperature etc. In case of data driven modelling approach, the controller does not require mathematical model of the plant and thus provides a better alternative solution than model-based control (Ayankoso and Habib 2020). Data

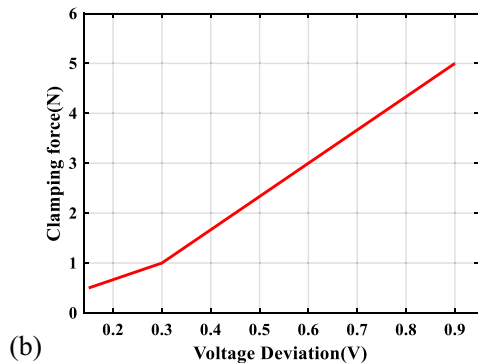
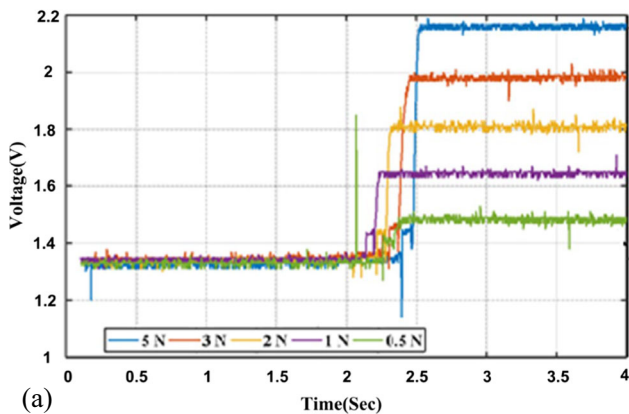


Fig. 7 a Voltage deviation vs time plot for different clamping forces applied on the stator of IM b Linear relationship of clamping force vs voltage deviation for clamping force measurement of the IM

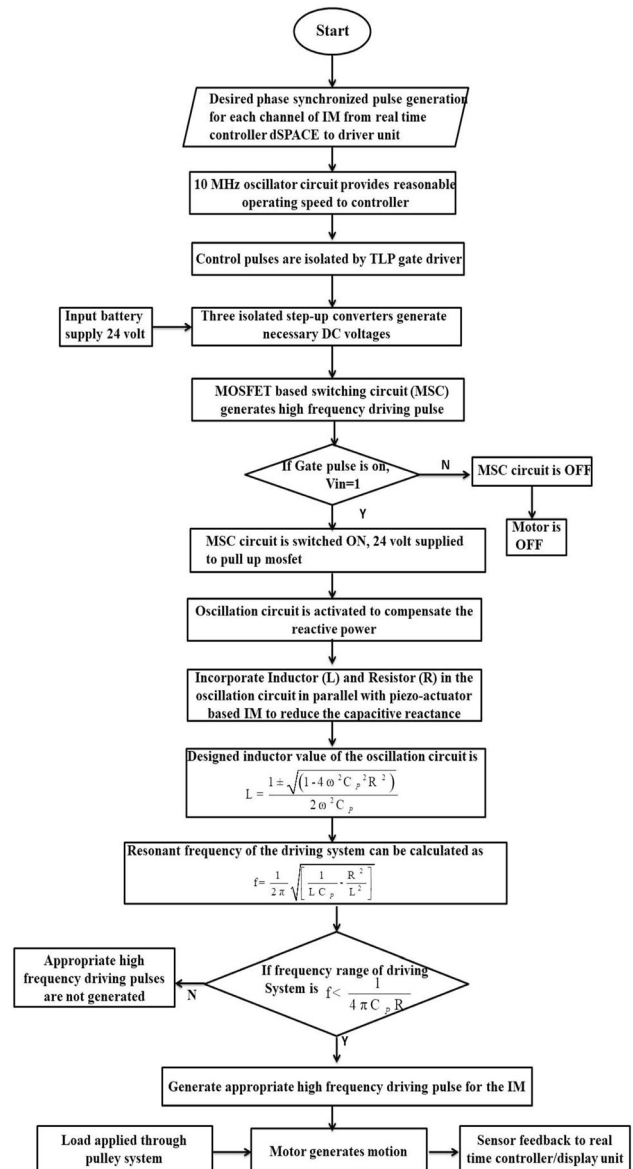


Fig. 8 Flow diagram of high frequency driving of the IM

driven model is more robust so that any variation of system performance can also be accounted by training (Barbosa et al. 2020; Reinhart and Steil 2016). Moreover, the system nonlinearity is approximated by the model parameter(s) through experimental data.

In this research, data driven model is developed for the piezo based linear inchworm motor using multi linear regression analysis. Experiments are carried out with different operating frequencies and experimental data from the motor is collected. The dataset of 20,000 population size consists of four independent parameters (voltage of clamp 1, voltage of extender, voltage of clamp 2 and time of operation) and one dependent or target parameter (displacement). The model is trained with 80% of the dataset and remaining 20% data's is used for testing purpose.

Experiments are conducted with individual frequency using linear multivariate regression model. The structure of regression function is represented as

$$d = a_1f_1 + a_2f_2 + a_3f_3 + a_4f_4 + b \tag{1}$$

where, 'f₂' and 'f₄' are clamp voltages and 'f₃' is extender voltage of the inchworm motor, 'f₁' is model operating time data, 'b' is an intersect point and 'd' is a displacement of the inchworm motor and 'a₁', 'a₂', 'a₃' and 'a₄' are model coefficients. For each case (different frequency data set), the model coefficients and R2 scores have been calculated, as tabulated in Table 2.

$$M_E = \frac{1}{n} \sum_{k=1}^n \left| \frac{e_k^a - e_k^m}{e_k^a} \right| \tag{2}$$

where, e_k^a = actual displacement e_k^m = model displacement.

Mean Absolute Percentage Error (MAPE) is calculated from Eq. 2 and plotted in Fig. 9. The MAPE is seen to be ranging from 5.23% for 10 Hz to 1.49% for 500 Hz frequency model. It can thus be concluded that error variation of the proposed model is within considerable range compared to experimental results, and hence the model can be extended for practical application.

Simulation and experimental results of the motor motion have been compared at frequencies of 10 Hz, 50 Hz, 100 Hz and 500 Hz under driving voltage of 100 V and clamping force of 8 N. The resultant waveforms show considerable concurrence between the experimental and simulation model which suggests an accurate modeling and good performance of the motor at different frequencies, as shown in Fig. 10. The motor displacement has been measured experimentally using laser displacement sensor as shown in Fig. 12c). It shows that with increase in frequency, the total measured displacement increases and the motor exhibits linearity when the driving frequency is varied from 10 to 500 Hz. Corresponding speed of the IM increases linearly from 0.03 mm/sec at 10 Hz to 1.235 mm/sec at 500 Hz. The displacement curve has more fluctuations when operated at low frequency (10–50 Hz) as compared to higher frequency due to decreases in system inductive reactance.

The degree of impact of extender voltage (f₃) in IM displacement is further elaborated in section IV. In order to improve the regression model accuracy, Eq. 3 has been considered as the regression function structure where 'f₃'

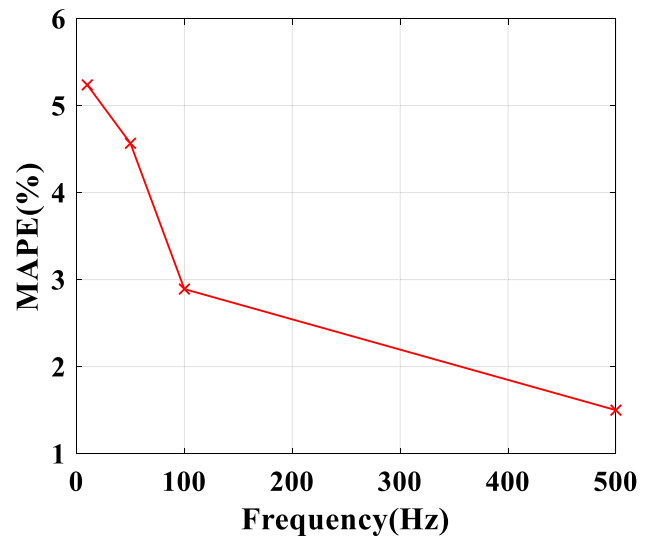


Fig. 9 MAPE error with different frequencies model

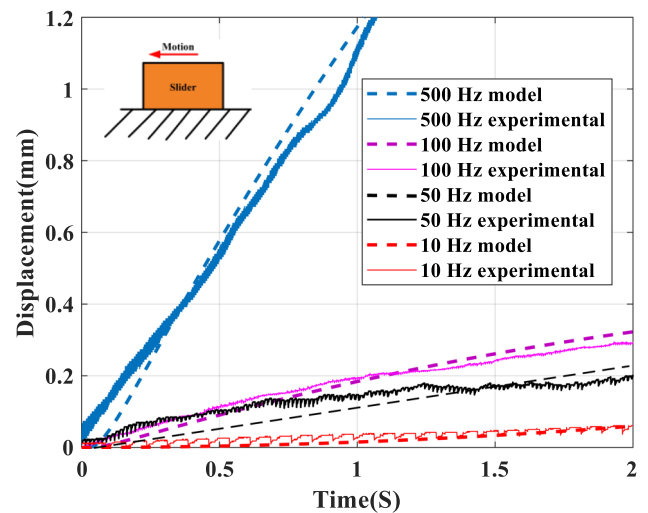


Fig. 10 Displacement vs time plot of inchworm motor with different frequencies under driving voltage of 100 V (simulation & experimental)

has an exponential term 'n'. With the variation of 'n', performances of regression model is demonstrated in Fig. 11. From the graph, it is found that the optimal value of 'n' for all frequencies model is found to be '1.6' where MAPE is minimum.

$$d = a_1f_1 + a_2f_2 + a_3f_3^n + a_4f_4 + b \tag{3}$$

Table 2 Co-efficient of regression model with different frequencies

Frequency	a ₁	a ₂	a ₃	a ₄	b	R2 score
500	4.089e-01	-1.267e-05	-1.370e-03	-4.215e-04	-1.392	0.968
100	4.089e-01	-1.267e-05	-1.370e-03	-4.215e-04	-1.392	0.548
50	2.922e-01	-5.870e-05	-2.025e-04	1.579e-04	-1.315	0.862
10	3.140e-01	-1.126e-04	2.945e-06	1.015e-04	-1.446	0.834

4 Piezoelectric inchworm motor characteristics experiments

4.1 Experimental setup

In order to test the design of the piezoelectric motor, series of experiments have been carried out. Figure 12 illustrates the experimental set-up of the prototype where Fig. 12a represents the signal flow diagram. Three appropriate phase synchronized control pulses have been generated from the control signal generator and high switching driver circuit is developed to drive the motor at a higher frequency. Desired output linear motion is generated by the motor when three amplified phase synchronized pulses are applied to the clamps and extender of the motor. A non-contact measurement laser displacement sensor (LK-G Series, KEYENCE) with a resolution of 20 nm is utilized to capture the motion. Using a pulley set up and standard weights, different loads are placed on the slider along the positive horizontal axis as shown in Fig. 12b and complete test bench set up under load is illustrated in Fig. 12c.

4.2 Experimental characterization of IM

4.2.1 Clamping error analysis

Clamping error of the inchworm motor has been calculated under free clamping force at no load condition and it is considered as clamp displacement along moving direction while two clamps are excited, keeping the extender in an unexcited state. When the actuator of clamping stack

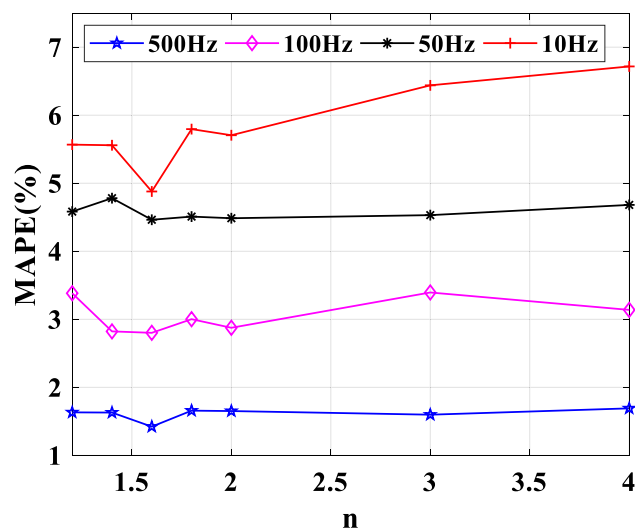


Fig. 11 Percentage of error change (MAPE) with variation of optimizing value 'n'

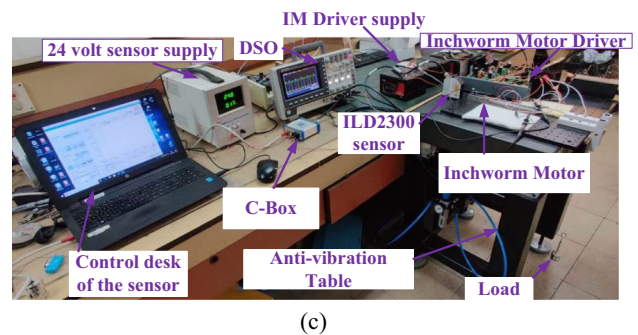
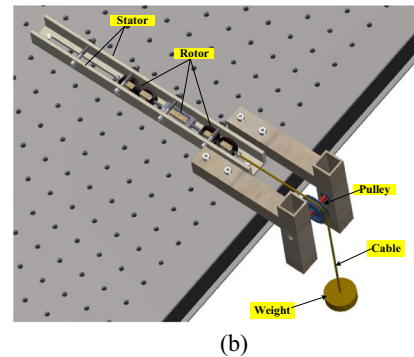
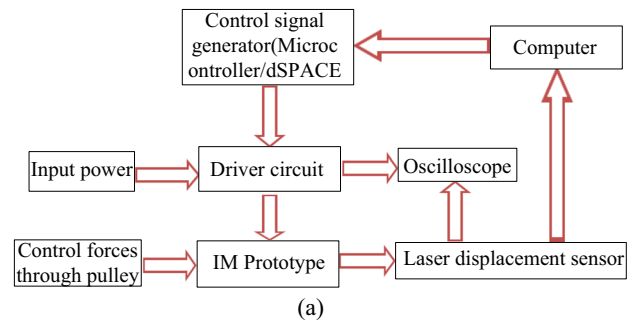


Fig. 12 Experimental test bench set up a Signal flow diagram b Schematic of load and pulley arrangement system c Experimental set up platform under load

alternately runs for 10 s with the extender untouched, the maximum movement recorded is quantitatively considered as clamping error. During the experiment, voltage ranges from 0 to 100 Volts under frequencies of 500 Hz, 1000 Hz, 2000 Hz resulted in maximum of 0.076542 mm, 0.11277 mm, 2.97 mm clamping errors respectively, which is mildly high for precise motion control as shown in Fig. 13a, b. Consequently, clamping voltage has been dynamically adjusted and kept between 20 to 40 V for 500 Hz, 40 V to 70 V for 1000 Hz and 60 V to 90 V for 2000 Hz in order to achieve optimal position accuracy. Clamp error is mainly caused by the lateral deviation and deflection of the extender, hence in order to reduce the clamp error, clamping voltage needs to be reduced and rigidity of the extender should also be increased.

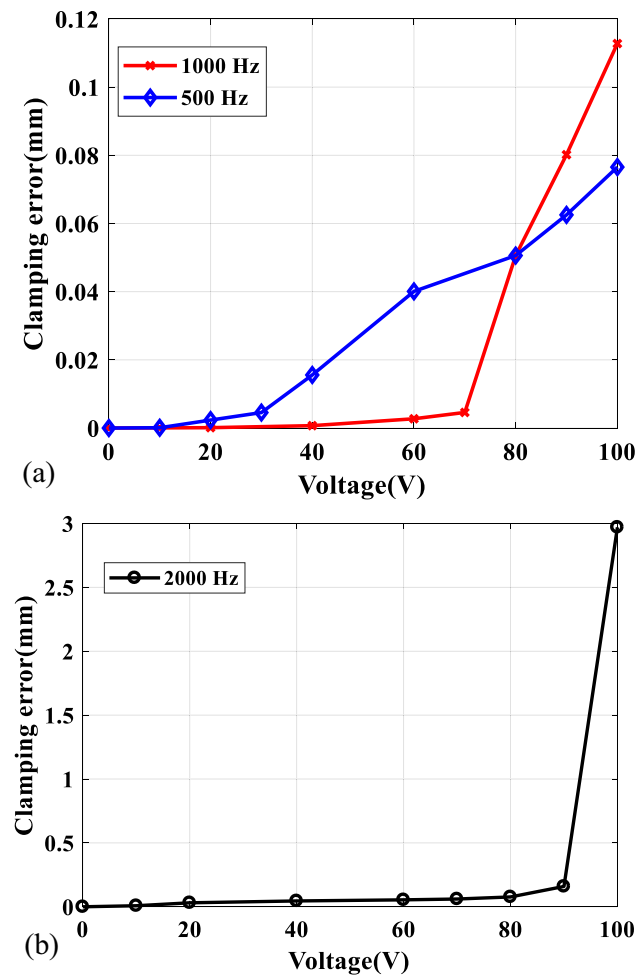


Fig. 13 Relationship between the clamping voltages with the clamping error with different frequencies a 1000 Hz, 500 Hz b 2000 Hz

4.2.2 Stability analysis with step length

Step length and displacement resolution plays an important role to determine performance of the inchworm motor. Step lengths are calculated by operating the motor with different driving voltages. However, it is also affected by some non-linear parameters such as clamping force, load, heat etc. At no load condition, it is observed that the relation between step length and driving voltage is linear as shown in Fig. 14a. Motor achieves maximum step length of 6.07 μm at no load condition under the clamping force of 5 N with driving voltage 100 V while the minimum step length of 0.817 μm is achieved at operating voltage of 20 Volt. The maximum stack displacement is 6.838 μm at 100 Volt driving voltage which is approximately equal to the motor step length. However, the motor stroke length is quite low in lower voltage range operation, being 0.817 μm under 20 Volt as compared to the nominal stack displacement of 1.668 μm. Thus, the motor’s nominal driving voltage must be greater than 20 Volt. Stability step length factor also

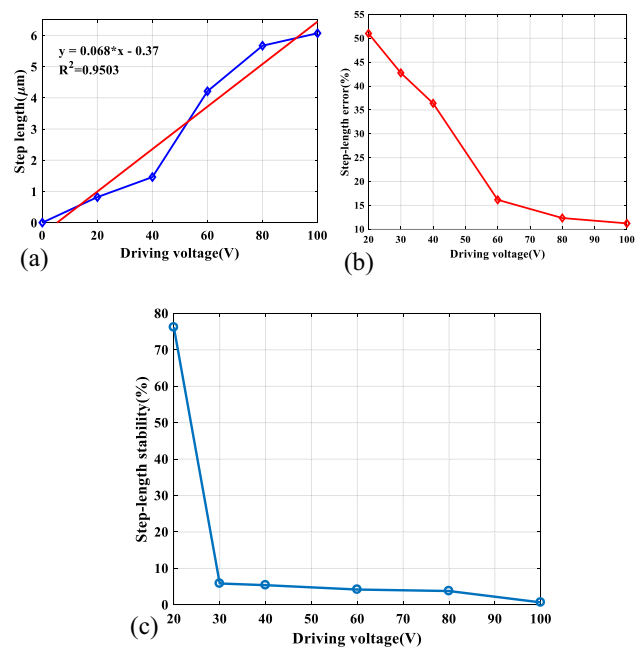


Fig. 14 a Step length vs driving voltage with frequency of 1000 Hz, b Relationship between step length error vs driving voltage c Relationship between step-length stability vs driving voltage of the IM

needs to be calculated in order to measure precise motion of the motor. Figure 14b shows the correlation between step length error and driving voltage. The error is seen to decrease slowly with increase in the driving voltage of the IM extender. The error associated with a driving signal of 100 Volt is found to be minimum of 11.23%, while the error associated with a 20 Volt signal is maximum at 51.01%. The result suggests the nominal voltage of the motor should be higher than 60 V in order to compensate the error.

Moreover, step-length stability is another key factor when evaluating movement precision. In this paper, the step length stability has been calculated using the Eq. 4 and relationship between step length stability and driving voltage is shown in Fig. 14c. It is found that the step length stability decreases gradually with increase in driving voltage with a best value corresponding to 100 Volts, being 0.67% of the actuator and the worst value corresponding to 20 Volts which is 72.6%. In order to increase the step length stability, the motor’s nominal voltage is recommended to be higher than 60 V.

$$\eta = \left(\sum_{k=1}^n \left| \frac{S_k - \bar{S}_n}{\bar{S}_n} \right| \right) / n \tag{4}$$

where, η is step length stability, S_k is actual step length of the inchworm motor, S_n is average step length of the motor after n steps and n is the no of steps.

4.2.3 Dynamic driving force

The motor output force is determined by combining thrust force generated by driving stacks with clamping force generated by clamping stacks. Clamping force is normally smaller than the driving force and the maximum output force is equal to the clamping force which is converted from the clamped of the IM. Continuous driving forces or dynamic driving forces are generated when an extender moves continuously with a load. The driving frequency and clamping voltage of the motor are set at 1000 Hz, 100 V respectively and the driving voltage of the extender is varied from 20 to 100 V.

As the driving voltage is increased, gradual increase in weight until the extender is out of step.

It is considered that under this driving voltage, the weight is defined as the maximum dynamic driving force. The relationships between dynamic force and driving voltage are seen in Fig. 15. During operating voltages between 10 and 60 V, the maximum dynamic driving force is found to increase linearly reaching about 1.8 Kgf at 60 V. After that, the dynamic force turns constant as the driving voltage is further increased and maximum driving force of 2.40 Kgf is achieved at 100 V.

4.3 Performance evaluation of IM

4.3.1 Voltage –speed characteristics

Figure 16 illustrates the relationship between the driving voltage and the output speed, where the driving frequency is 1000 Hz. Speed of the motor increases linearly with increasing the excitation voltage of the extender. The motor achieves a maximum speed of 17.28 mm/s for a voltage of 100 V driving pulse when a clamping force of 2

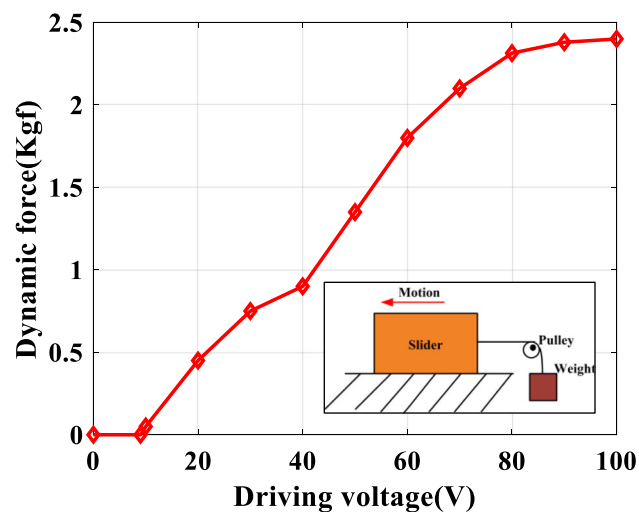


Fig. 15 Relationship between dynamic force vs driving voltage

N is applied. The resultant IM speed is found to inversely proportional to the clamping force and directly proportional to the extender excitation voltage.

4.3.2 Frequency- speed/step length characteristics

Figure 17 illustrates the relationship between driving frequency and speed when different clamping forces (2 N, 5 N, 8 N) are applied to the motor rail. With an increase in driving frequency, speed of the motor increases linearly, but after a frequency of 2000 Hz, the increase in speed reduces. Here, the piezo-actuator's capacitive effect might be in play, and the piezo stack does not have enough time to extend to its theoretical length. In this experiment, excitation voltage for the motor is 100 Volt square pulses at 30% duty cycle. At a driving frequency and voltage of 2000 Hz and 100 V, a maximum speed of 39.64 mm/s is achieved when the clamping force is 2 N. The motor speed falls from 39.64 to 10.40 mm/s when clamping force of 8 N is applied to the motor rail through clamping screw as shown in Fig. 12b. The result suggests the maximum motor speed is reached when it operates at 2000 Hz driving input voltage, so the motor runs in its optimal condition at this frequency. Based on the results of the experimental set up, it can be observed that the piezo-based inchworm motor exhibits a stable operation. Accordingly, the frequency of 2000 Hz has been considered as the optimal working frequency and considered for further experiments, detailed in subsequent sections.

The motor's step lengths have been measured at frequencies between 100 and 2500 Hz under clamping forces of 2 N, 5 N and 8 N with a voltage of 100 V. Figure 18 indicates that when the frequency increases, step length of the motor under different clamping forces initially increase, and then decreases.

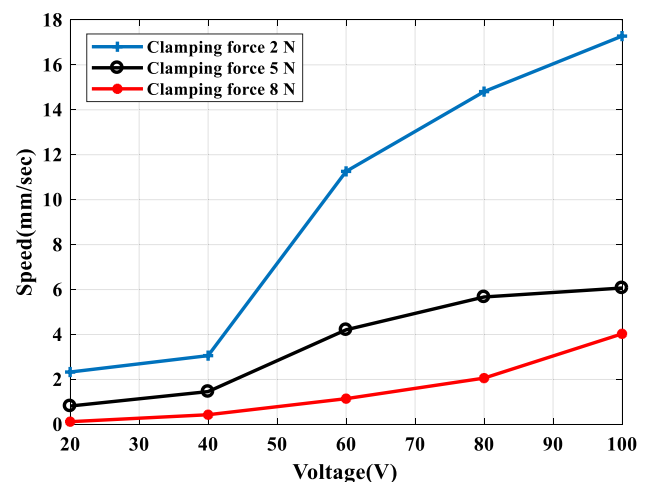


Fig. 16 Relationship between the extender driving voltage and speed of the IM with different clamping forces at 1000 Hz frequency

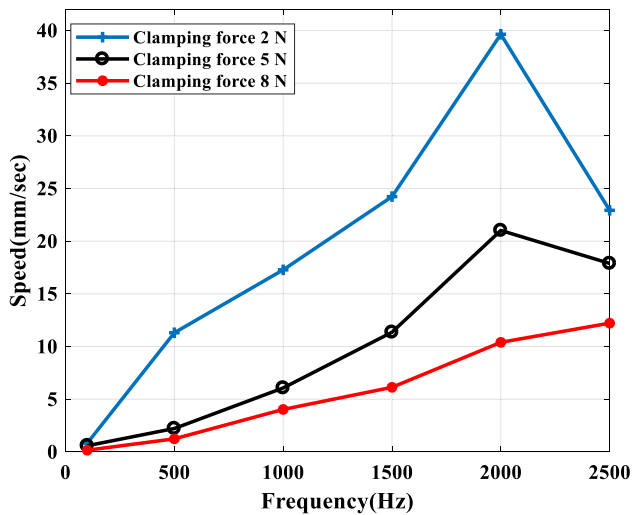


Fig. 17 Relationship between the driving frequency and speed of the motor with different clamping forces

Maximum step length of 22.62 μm , 4.44 μm , 2.48 μm is achieved under clamping force of 2 N, 5 N, 8 N respectively at frequency of 500 Hz. As discussed earlier, for optimal operation of the motor, the step length increases at a frequency of 2000 Hz.

4.3.3 Speed-load characteristics

The load along the horizontal axis of the motor is measured with different standard weights. The correlation between the working load and output speed under the variation of clamping forces is illustrated in Fig. 19. It is observed that speed of the motor decreases as the load increases. In this experimental study, the operating frequency and duty cycle of driving pulse are 2000 Hz and 30% respectively and magnitude of the voltage is about 100 Volt. The maximum

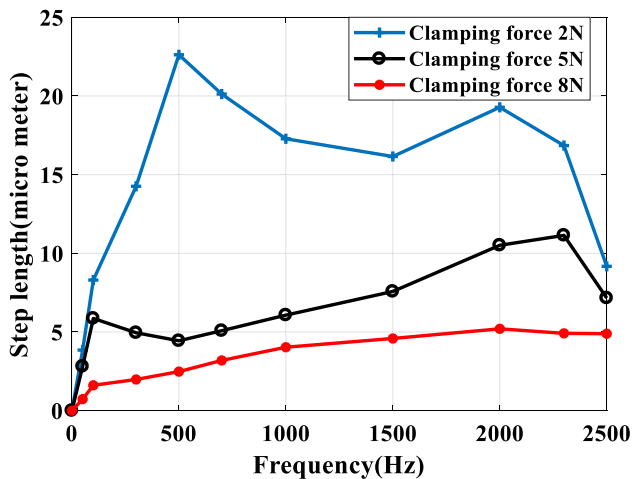


Fig. 18 Relation between step length and frequency of the IM with different clamping forces

loads are 1.71 N, 4.41 N, 6.86 N under clamping forces 2 N, 5 N, 8 N during the experiment. The no load speed of the motor drops from 39.64 to 19.75 mm/s due to load of 50 gm under clamping force of 2 N. This might explain the pre-loading gap and the tolerance values of the motor rail as output speed vs load does not follow linear characteristics.

4.3.4 Impact on speed with and without load

In the experimental work, inchworm motor is operated with 100 Volts driving pulses and tested at different frequencies of 100 Hz, 500 Hz, 1000 Hz, 1500 Hz, 2000 Hz, and 2500 Hz, respectively. A weight of 2 N is attached to the motor rotor and clamped with a thrust of 5 N. Regardless of whether the motor is loaded or not, the speed of the motor increases with increasing frequency, up to 2000 Hz. Highest speed of 3.79 mm/sec is achieved under a load of 2 N at a frequency of 2000 Hz as shown in bar diagram Fig. 20. The driving pulse's duty cycle leads to a speed decrease of 2.54 mm/sec under frequency of 2500 Hz. Thus, to increase the load capacity and speed, a reduction in the duty cycle is undertaken.

4.3.5 Three phase voltage waveform pattern across the IM at different frequency operation

Three phase synchronized voltages applied across the two clamps and extender of the motor are seen in Fig. 21 where voltage magnitude of the motor [clamp 1, extender, clamp 2] increases from [40 V, 52 V, 48 V] to [74 V, 94 V, 80 V] as frequency increases from 10 to 500 Hz. It is observed that at a very low frequency (10 Hz), there is a certain peak that decreases with increasing the switching frequency of the driving input signal. This may be due to

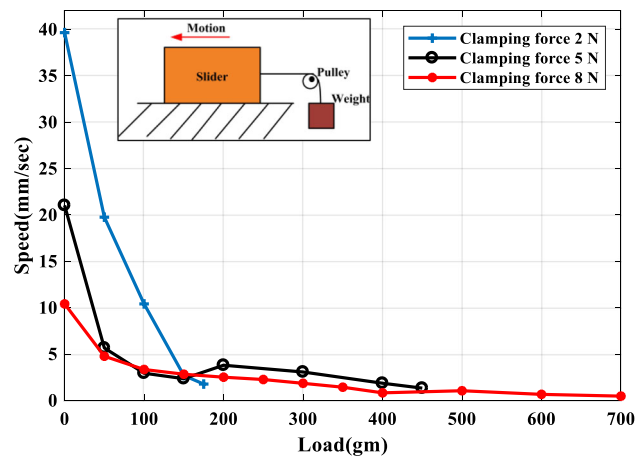


Fig. 19 Relationship between the load variation and speed of the motor with different clamping forces

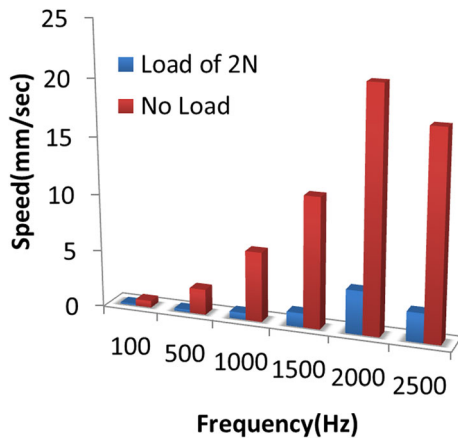


Fig. 20 Variation of frequency as a function of speed with and without loading

combined effect of presence of capacitance of piezo-actuator and the designed driver circuit. With an increase of driving frequency, the voltage magnitude increases as the inductive reactance of the driving circuit rises, so the current drawn from the driving circuit reduces due its to power limitation.

Analyzing the results, it is found that the inchworm motor exhibits superior stability at high frequencies than at lower frequency operation.

Due to this, inchworm motors can drive at high voltage and high frequency while maintaining step length stability and speed making it suitable for high speed operation. However, the motor’s clamping voltage should be kept within the identified frequency dependent voltage range (as discussed in section IV) in order to reduce the clamping error.

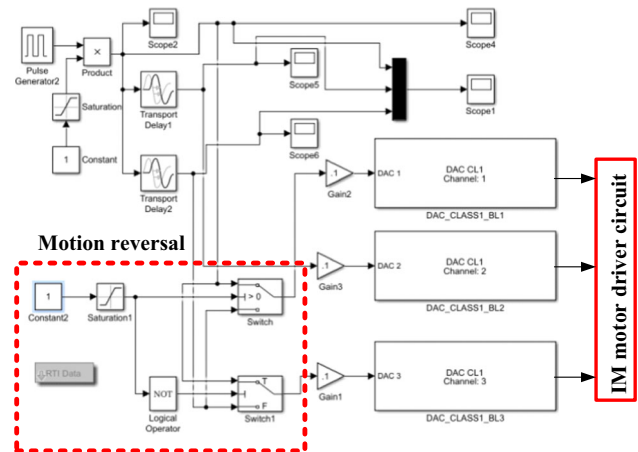


Fig. 22 Motion direction reversal model in dSPACE

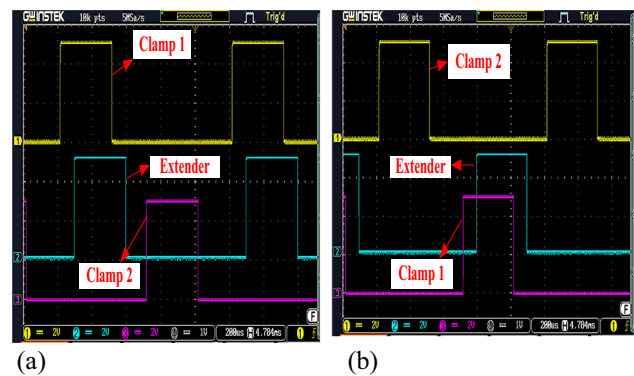


Fig. 23 Piezoelectric IM direction reversal control signals a forward motion b reverse motion

5 Forward and reverse motion of IM

Direction reversal control pulse generation logic has been developed in MATLAB Simulink and interfaced with real time digital controller platform, dSPACE 1202 to drive the IM in forward and backward direction. As shown in Fig. 22, two transport delay blocks are used to get the desired three phase- shifted control pulses necessary to achieve synchronization between the two clamps and extender to ensure smooth operation of the IM. Two switches are used to interchange the clamp signals for forward and reverse direction of the motor at any instant which is determined by the value of a constant block preceding the switch. The motion reversal control pulses of the IM are seen in Fig. 23, comprising two 180 degree out of phase signals for the clamps which are reversed depending in direction of motion control. At no load condition, the inchworm motor’s forward and backward motion is verified at frequencies of 10 Hz and 1500 Hz under driving signals of 100 Volts and clamping forces of 4 N, as shown in Fig. 24. A displacement vs time plot of

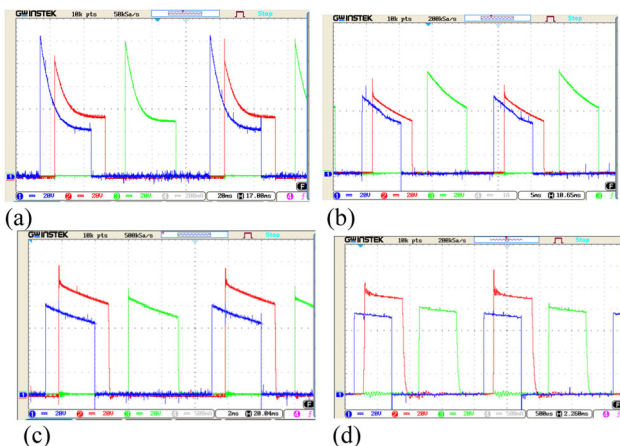


Fig. 21 Voltage measurement plot across IM in DSO at different frequencies (clamp 1 (blue), extender (red), clamp 2 (green)) a 10 Hz, b 50 Hz, c 100 Hz and d 500 Hz

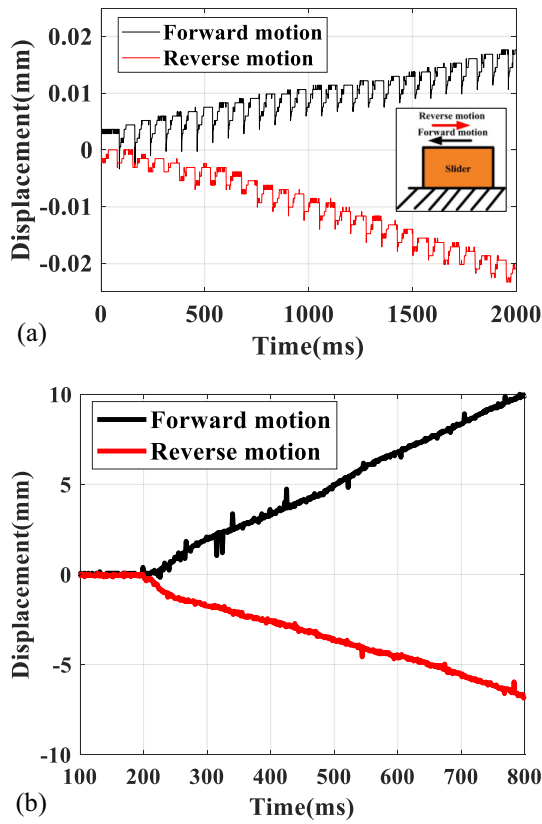


Fig. 24 **a** Bidirectional motion of the IM at low frequency input signal, 10 Hz **b** Bidirectional motion of the IM at high frequency input signal, 1500 Hz

bidirectional linear motion of the inchworm motor (frequency of 1500 Hz) is shown in Fig. 24b where the motor moves 10 mm in forward and 6.5 mm in backward directions. The average speeds for forward and backward

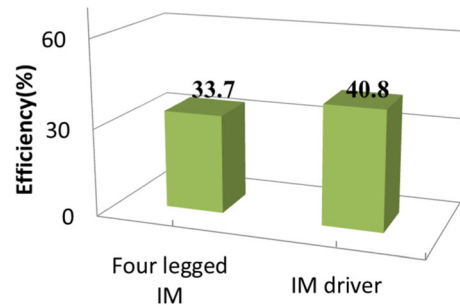


Fig. 25 Efficiency plot of the IM

motion at 1500 Hz are 16.66 mm/s and 11.66 mm /sec respectively.

Table 3 represents a comparison between the proposed work and the previous works. In terms of operating frequency, speed, output load capacity, clamping force, the proposed motor has obvious advantages. With a clamping force of 8 N, the maximum load capacity of the proposed motor is 700 gm, while the operating frequency 2500 times previous research(Ghenna et al. 2023) and maximum load capacity is 17.5 times higher than in ref Pan et al. (2023). Compared to other piezoelectric mechanisms reported to date, the four-legged Inchworm motor features a higher operation frequency, motion range, speed, and load capacity.

The output and input power of the electrical driver circuit are used to determine the electrical driver and mechanical efficiency of the IM, as shown in bar diagram, Fig. 25. Mechanical efficiency of the motor has been derived under load of 2 N. In the experimental measurements, the efficiency of the IM is found to be 33.7% at 100 V and 2 kHz operating frequency which is much better

Table 3 Comparison between the proposed work and the previous reported work

Piezo-actuator based IM	Frequency[Hz]	Voltage[V]	Maximum speed [mm/sec]	Maximum load [gm]	Maximum clamping force [N]	Efficiency [%]	Motion range [mm]	Step displacement [μ m]
Jie Ling (2022)	650	80	44.69	60	432.2	Low	4.3	71
Jianping Li (2017)	1000	100	7.95	158	NA	NA	0.1	11.52
By Tinghai Cheng (2017)	500	100	5.96	300	5	NA	0.130	NA
I. Penskiy (2011)	600	110	3.6	NA	0.0007	17	0.06	NA
H.Dong (2020)	50	120	0.72	NA	NA	Low	11	NA
S. Ghenna (2023)	1	80	0.00225	-	300N	NA	0.01	NA
J.Ma (2023)	500	100	2.287	500	NA	NA	10	8.94
Q. Pan (2023)	752	82.4	11.14	40	15	NA	0.15	0.5
Proposed work	2500	100	39.64	700	8	33.7	90	22.62

than the 17% measured for electrostatic inchworm motors at 110 Volts and 600 Hz frequency (Penskiy et al. 2011).

6 Conclusion

In this research paper, a high force piezo based linear inchworm motor with bidirectional motion is proposed, designed, fabricated and tested. The four-legged motor comprises two clamps each consisting of two piezoelectric stack actuators and an extender which brings about the displacement. After mechanical design and force evaluation of the constituent components, the working prototype has been fabricated and tested by driving the motor with three appropriate phase shifted and synchronized control pulses applied to the clamps and extender. For enhanced control, a regression model of the motor has been developed from experimental data which reduces error commonly associated with variations in operating conditions and presence of non-linearities. Comparison of the experimental motor output with that of the simulation model reveals a good agreement and shows that the model could achieve a linear operation in high frequency range. A maximum step-length of 22.62 μm is achieved under 100 V, with a displacement resolution of 0.817 μm under 20 V. In order to ensure step stability, the minimum driving voltage is found to be 60 V and clamp voltage should remain within the identified range to reduce clamping error. Several experiments have been carried out to evaluate the performance of the motor viz. displacement at different operating voltage, driving frequency, clamping force and loading effects. The amount of clamping force acting on the clamps of the motor rail plays an important role for driving the motor and has been measured using load cell. Logic for real time, bidirectional motion of the proposed inchworm motor has also been designed and the motor achieves a uniform speed in both forward and reverse directions. The speed increases with increasing the driving frequency however after 2000 Hz, the speed is seen to decrease which can be compensated by reducing the duty cycle of the actuating pulse. This can be the result of mechanical slipping due to retraction forces being higher than clamping force. A performance limitation is restricted frequency of operation as piezoelectric actuator capacitance dynamically varies with frequency, an upper threshold needs to decide which can be electrically balanced through appropriate driver circuit. Further improvements can be carried out in the driving circuit by electrically balancing the piezo-actuator's reactance, specifically at high frequencies and which may also reduce the oscillation of the motion.

Acknowledgements The authors gratefully acknowledge collaboration between CSIR-India, Centrale Supélec and Faurecia funded by the Indo-French Centre for the Promotion of Advanced Research (IFCPAR/CEFIPRA) under the grant number IFC71123 and S.J thanks CSIR HRDG, India for providing CSIR-SRF fellowship to carry out his research work with grant number 31/0019(11388)/2021-EMR-I.

Author contributions SJ and SKS conceived the idea. SKS designed the research methods. SJ designed and developed the motor and driver circuit. SJ and SKS wrote the manuscript. AKN conceived the idea of data data-driven modeling approach. All authors contributed to the editing and revision of the manuscript. The authors read and approved the final manuscript.

Funding The authors gratefully acknowledge the funding received from the Indo French Center for the Promotion of Advanced Research (IFCPAR/CEFIPRA) for carrying out this work.

Data availability No datasets were generated or analysed during the current study.

Declarations

Conflict of interest The authors declare no conflict of interest.

References

- Ayankoso SA, Habib MK (2020) Data-driven modeling of a two-link flexible manipulator (TLFM), 2020 21st International Conference on Research and Education in Mechatronics (REM). 1–6, <https://doi.org/10.1109/REM49740.2020.9313894>
- Barbosa MPS, Rakotondrabe M, Ayala HVH (2020) Deep learning applied to data-driven dynamic characterization of hysteretic piezoelectric micromanipulators. *IFAC-Papers on Line* 53(2):8559–8564
- Calkins FT, Smith RC, Flatau AH (2000) An energy-based hysteresis model for magnetostrictive transducers. *IEEE Trans Magn* 36(2):429–439
- Cheng T, He M, Li H, Lu X, Zhao H, Gao H (2017) A Novel trapezoid-type stick–slip piezoelectric linear actuator using right circular flexure hinge mechanism. *IEEE Trans Industr Electron* 64(7):5545–5552. <https://doi.org/10.1109/TIE.2017.2677318>
- Cusin P, Sawai T, Konishi S (2000) Compact and precise positioner based on the Inchworm principle. *J Micromech Microeng* 10:516–521
- Devasia S, Eleftheriou E, Moheimani R (2007) A survey of control issues in nanopositioning. *IEEE Trans Control Syst Technol* 15(5):205–213. <https://doi.org/10.1109/TCST.2007.903345>
- Dong H, Li T, Wang Z, Ning Y (2020) Design and experiment of a piezoelectric actuator based on inchworm working principle. *Sens Actuators A: Physical* 306:111950. <https://doi.org/10.1016/j.sna.2020.111950>
- Galante TP, Frank JE, Bernard J, Chen W, Lesieutre GA, Koopmann GH (1998) Design, modeling, and performance of a high-force piezoelectric inchworm motor, *Proc. SPIE 3329, Smart Structures and Materials: Smart Structures and Integrated Systems*. <https://doi.org/10.1117/12.316945>
- Ghenna S, Bernard Y, Daniel L (2023) Design and experimental analysis of a high force piezoelectric linear motor. *Mechatronics* 89:102928

- Joshi CH (2020) Compact magnetostrictive actuators and linear motors, Proc.7th International Conference on New Actuators Bremen, Germany, pp.120–125
- Kim JW, Kim JD, Choi SB (2002) A hybrid inchworm linear motor. *Mechatronics* 12:525–542
- Li J et al (2017) Development of a novel parasitic-type piezoelectric actuator. *IEEE/ASME Trans Mechatron* 22(1):541–550. <https://doi.org/10.1109/TMECH.2016.2604242>
- Ling J, Chen L, Feng Z, Zhu Y (2022) Development and test of a high speed pusher-type inchworm piezoelectric actuator with asymmetric driving and clamping configuration. *Mech Mach Theory* 176:104997. <https://doi.org/10.1016/j.mechmachtheory.2022.104997>
- Ma J et al (2023) An inchworm and stick-slip dual mode piezoelectric linear actuator for cell injection. *IEEE Access* 11:70534–70541. <https://doi.org/10.1109/ACCESS.2023.3285271>
- Makarem S, Delibas B, Koc B (2021) Data-Driven tuning of PID controlled piezoelectric ultrasonic motor. *Actuators* 10:148. <https://doi.org/10.3390/act10070148>
- Nabavi S, Zhang L (2018) Design and optimization of a low-resonant-frequency piezoelectric MEMS energy harvester, Based on Artificial Intelligence; Proceedings. 2: 930.
- Pan Q, Huang F, Chen J, He LG, Li W, Feng Z (2017) High-speed low-friction piezoelectric motors based on centrifugal force. *IEEE Trans Industr Electron* 64(3):2158–2167. <https://doi.org/10.1109/TIE.2016.2623578>
- Pan Q, Huang Z, Zhao M, Chen L, Huang Q, Li R (2023) Development of a dual-stator piezoelectric motor operated in resonance and quasi-static states. *Mech Syst Signal Process* 183:109618. <https://doi.org/10.1016/j.ymsp.2022.109618>
- Penskiy I, Bergbreiter S (2013) Optimized electrostatic inchworm motors using a flexible driving arm. *J Micromech Micro Eng* 23(1):015018. <https://doi.org/10.1088/0960-1317/23/1/015018>
- Penskiy I, Gerratt AP, Bergbreiter S (2011) Efficient electrostatic inchworm motors with simple control and high force density, 2011 16th International Solid-State Sensors, Actuators and Microsystems Conference. 24382441, <https://doi.org/10.1109/transducer.2011.5969660>.
- Reinhart RF, Steil JJ (2016) Hybrid mechanical and data-driven modeling improves inverse kinematic control of a soft robot. *Procedia Technol* 26:12–19. <https://doi.org/10.1016/j.protyc.2016.08.003>
- Shi Y, Sun H, Cheng D, Zhang J, Lin Y, Sun H (2021) A hybrid linear actuator based on screw clamp operation principle: design and experimental verification. *J Intell Mater Syst Struct*. <https://doi.org/10.1177/1045389X211064322>
- Sintov A, Kimmel A, Wen B, Boularias, Bekris K (2020) Tools for data-driven modeling of within-hand manipulation with under-actuated adaptive A. hands. *Proc Mach Learn Res* 120:771–780
- Xing J, Qin Y (2020) A novel low-frequency piezoelectric motor modulated by an electromagnetic field. *Actuators* 9:85
- Xu D, Liu Y, Shi S, Liu J, Chen W, Wang L (2018) Development of a nonresonant piezoelectric motor with nanometer resolution driving ability. *IEEE/ASME Trans Mechatron* 23(1):444–451. <https://doi.org/10.1109/TMECH.2018.2790923>
- Yamamoto Y, Eda H, Shimizu J (1999) Application of giant magnetostrictive materials to positioning actuators, Proc. IEEE/ASME of International Conference on Advanced Intelligent Mechatronics Atlanta, USA, pp.215–220.
- Yang BT, Bonis M, Tao H, Prella C, Lamarque F (2006) Magnetostrictive mini actuator for long-stroke positioning with nanometer resolution. *J Micromech Microeng* 16:1227–1232

Publisher's Note Springer Nature remains neutral with regard to jurisdictional claims in published maps and institutional affiliations.

Springer Nature or its licensor (e.g. a society or other partner) holds exclusive rights to this article under a publishing agreement with the author(s) or other rightsholder(s); author self-archiving of the accepted manuscript version of this article is solely governed by the terms of such publishing agreement and applicable law.